

Crossover of the three-dimensional topological insulator Bi_2Se_3 to the two-dimensional limit

Ke He, Qi-Kun Xue *et al.**

A topological insulator^{1–9} is a new state of quantum matter that is characterized by a finite energy gap in the bulk and gapless modes flowing along the boundaries that are robust against disorder scattering. The topological protection of the surface state could be useful for both low-power electronics¹⁰ and error-tolerant quantum computing^{11,12}. For a thin slab of three-dimensional topological insulator, the boundary modes from the opposite surfaces may be coupled by quantum tunnelling, so that a small, thickness-dependent gap is opened up^{13–15}. Here we report such results from angle-resolved photoemission spectroscopy on Bi_2Se_3 films of various thicknesses grown by molecular beam epitaxy. The energy gap opening is clearly seen when the thickness is below six quintuple layers. The gapped surface states also exhibit sizeable Rashba-type spin-orbit splitting because of the substrate-induced potential difference between the two surfaces. The tunable gap and the spin-orbit coupling make these topological thin films ideal for electronic and spintronic device applications.

Bi_2Se_3 , along with the congeneric Bi_2Te_3 and Sb_2Te_3 , is theoretically predicted^{16,17} and experimentally observed^{17–19} to be a three-dimensional (3D) topological insulator with a single Dirac cone. For possible applications of the topological insulators, planar devices would be most promising. Thin films of Bi_2Se_3 have been grown by molecular beam epitaxy²⁰ (MBE) and by the vapour–liquid–solid method in nanoribbon form²¹. Finite-size effects have to be considered for a topological insulator film of only several nanometres. For both 2D (ref. 22) and 3D (refs 13–15) topological insulators, the finite-size effects were studied theoretically within the effective models of refs 3, 16, and by first-principles calculations¹⁶. Owing to the coupling between the surface states, a finite energy gap is predicted to open in the 2D limit of the 3D topological insulators. Furthermore, the 2D energy gap is predicted to oscillate between the ordinary insulator gap and the quantum spin Hall (QSH) gap as a function of thickness. In this work, by combining MBE, angle-resolved photoemission spectroscopy (ARPES) and model calculations, we have systematically studied the thickness-dependent evolution of the band and spin structure of 3D topological insulator Bi_2Se_3 film with a thickness from one quintuple layer (QL) to 50 QL.

Figure 1a and b show the reflection high electron diffraction (RHEED) pattern and a scanning tunnelling microscope (STM) image of a typical MBE-grown Bi_2Se_3 film with a thickness of 50 QL, respectively. The sharp 1×1 streaks and atomically flat morphology demonstrate the high crystal quality of the film. Figure 1c shows the band map of the film. The bands show similar structure and dispersion to bulk Bi_2Se_3 (ref. 17). Two bands with nearly linear dispersion cross each other at the $\bar{\Gamma}$ point, forming a Dirac cone. They are the gapless surface states of Bi_2Se_3 . The band map shown in Fig. 1c does not exhibit the conduction band like

in the bulk samples¹⁷. The Dirac point is located at 0.12 eV below the Fermi level. The observation indicates that our MBE-grown Bi_2Se_3 samples are a nearly intrinsic topological insulator with a single Dirac point and contain fewer impurities, compared with the bulk samples^{17,23}.

By delicate control of the growth condition, we were able to achieve QL-by-QL growth of the Bi_2Se_3 thin films. Figure 1d shows a series of normal emission spectra of Bi_2Se_3 films from 1 to 6 QL with a step of ~ 0.3 QL. The peaks indicated by broken vertical bars are quantum well states (QWSs) of the valence band, which will be addressed later. With increasing thickness, a stepwise change in the QWS peaks is clearly observed in Fig. 1d, which indicates a QL-by-QL growth mode²⁴. It enables us to investigate the thickness-dependent band structures of the Bi_2Se_3 films with an accuracy of 1 QL.

Figure 2a–e shows a series of ARPES band maps of Bi_2Se_3 films from 1 to 6 QL (except for 4 QL) measured at room temperature. All of the spectra are taken along the $\bar{\Gamma}-\bar{K}$ direction. The spectra of 1 QL (Fig. 2a) exhibit a nearly parabolic band dispersion towards the Fermi level along k_{\parallel} . At 2 QL (Fig. 2b), the band moves down by 40 meV and another band appears below it. As shown later, the two bands finally evolve into the gapless surface states in thicker films. We refer to them hereafter as the upper and lower surface states, respectively, although the distinction between the surface and bulk states is blurred in films this thin. At 3 QL (Fig. 2c), the gap between the upper and lower surface states decreases. Interestingly, the upper surface states are split into two branches. The splitting is more prominent at larger wavevectors but disappears at the $\bar{\Gamma}$ point as shown in the energy distribution curves (EDCs) in Fig. 2f. This is a Rashba-type splitting, in which the two sub-bands with different spins shift along the k_{\parallel} axis in opposite directions and degenerate at the $\bar{\Gamma}$ point. For thicker films at 5 and 6 QL (Fig. 2d,e), the gap between the two surface states decreases further. Meanwhile, the outer two branches of the split upper surface state fade out gradually. At 6 QL, the gap disappears and so do the outer branches of the upper surface states. The inner branches of the upper surface states connect the lower surface states, resulting in a Dirac cone (Fig. 1c).

The Dirac point at 6 QL is located at -0.26 eV, lower by 0.14 eV than that of the thick (50 QL) Bi_2Se_3 films shown in Fig. 1c. It suggests that the film is electron doped. Above 6 QL, the Dirac point moves towards the Fermi level with increasing thickness until ~ 20 QL where the saturation value is reached. Figure 3a plots the thickness dependence of the Dirac point position. For comparison, the measured mid-gap energies of the surface states and the spin-degenerate points of the Rashba-split upper surface states are also shown. As STM experiments show little difference in surface defect density between thick and thin films, the thickness-dependent electron doping may come from band bending resulting from charge transfer from the SiC substrate.

*A full list of authors and their affiliations appears at the end of the paper.

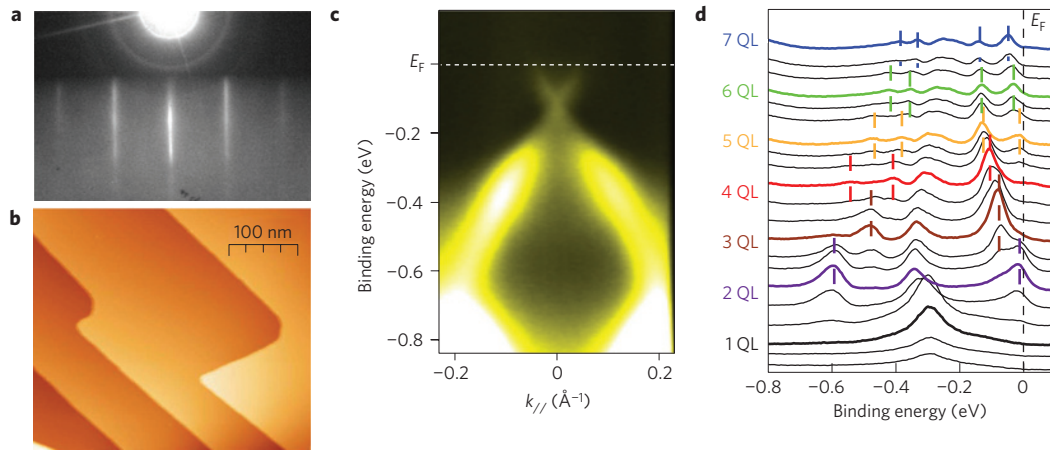


Figure 1 | Growth of Bi₂Se₃ films. **a**, RHEED pattern of a 50 QL Bi₂Se₃ film grown by MBE. **b**, STM image of the film. **c**, ARPES spectra of the film along the Γ - \bar{K} direction. **d**, Thickness-dependent normal emission photoemission spectra of Bi₂Se₃ films. The thickness step is ~ 0.3 QL.

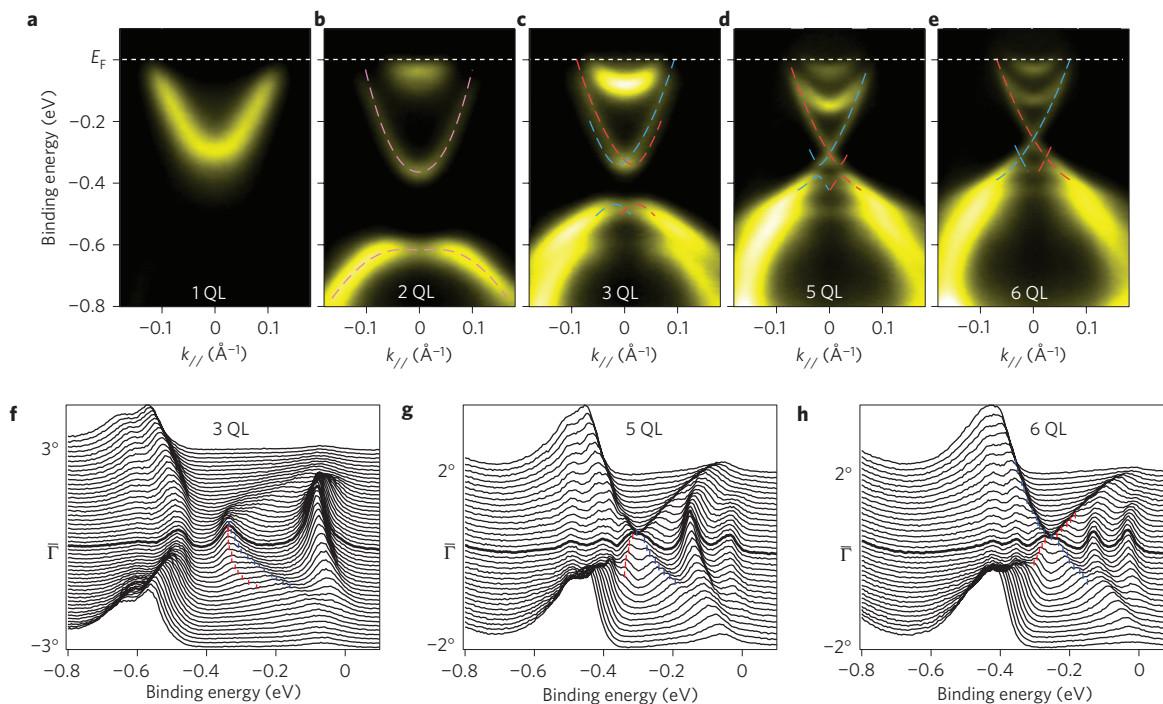


Figure 2 | ARPES spectra of Bi₂Se₃ films at room temperature. **a-e**, ARPES spectra of 1, 2, 3, 5 and 6 QL along the Γ - \bar{K} direction measured at room temperature. **f**, EDCs of **c**. **g**, EDCs of **d**. **h**, EDCs of **e**. The pink dashed lines in **b** represent the fitted curves using equation (1). The blue and red dashed lines in **c-e** represent the fitted curves using equation (2). The corresponding fitting parameters are listed in Table 1.

Besides the surface states, above 2 QL, there are other features either above the upper surface states or below the lower surface states. With increasing thickness, these bands move up or down towards the surface states, and more bands emerge. In Fig. 3b we summarize the energies of these bands at the Γ point with respect to the mid-gap energies of the surface states. The mid-gap energies are used as a reference to remove the influence of chemical potential change. The energy evolution shows a typical QWS behaviour. Therefore, these bands can be attributed to QWSs of conduction and valence bands.

When the thickness of a film is reduced to only several nanometres, overlapping between the surface-state wavefunctions from the two surfaces of the film becomes non-negligible, and hybridization between them has to be taken into account. For a freestanding and symmetric Bi₂Se₃ film, the spin-polarized surface states at one surface will be mixed up with the components of

opposite spin from the other surface when the thickness is small enough. It will lead to a hybridization gap at the Dirac point to avoid crossing of bands with the same quantum numbers. The observed gap opening below 6 QL can preliminarily be attributed to this effect. The band and spin structures of a 3D topological insulator such as Bi₂Se₃ near the Fermi level are well described by the four-band effective model¹⁶. In the ultrathin limit¹⁵, the 3D topological insulator model of ref. 11 reduces to the Bernevig–Hughes–Zhang model³ of the 2D QSH insulator, and the in-plane dispersions of the surface states can be written as¹⁵:

$$E_{\pm}(k_{//}) = E_0 - Dk_{//}^2 \pm \sqrt{(v_F \hbar k_{//})^2 + \left(\frac{\Delta}{2} - Bk_{//}^2\right)^2} \quad (1)$$

The term including the Fermi velocity v_F is the Dirac component of the bands, and Δ represents the gap size. The definition of

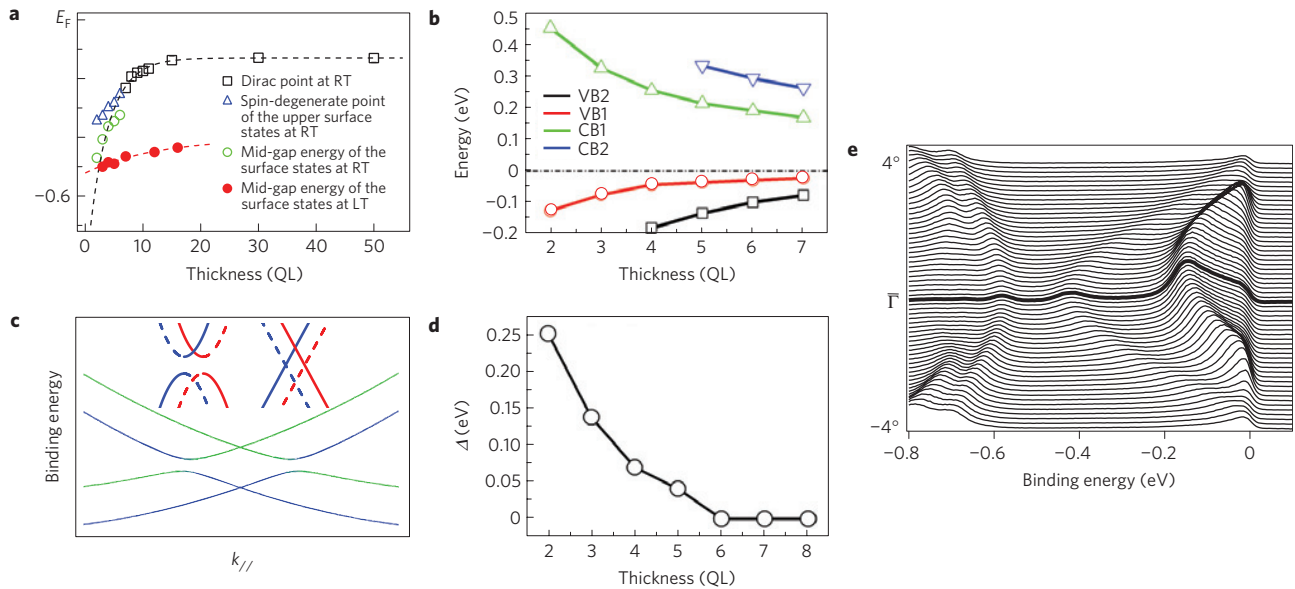


Figure 3 | Analyses of the ARPES data of Fig. 2. **a**, Thickness dependence of the binding energies of the Dirac point (≥ 6 QL) (open black squares), the spin-degenerate point (< 6 QL) (open blue triangles) and the mid-gap position E_0 of the surface states (< 6 QL) measured at room temperature (RT; open green circles) and 150 K (low temperature (LT); filled red circles). **b**, Thickness-dependent energies of QWS peaks at the Γ point relative to the mid-gap energy E_0 . **c**, Real-space weight of the surface states at 5 QL. The green and blue colours represent the states that mainly localize at the surface and interface, respectively. The inset shows a schematic illustration of the surface states of a Bi_2Se_3 film above (right) and below (left) 6 QL. The solid and dashed lines represent the surface states that mainly localize at the surface and interface of the Bi_2Se_3 film, respectively. The red and blue colours of the lines represent different spins. **d**, Thickness dependence of the measured gap size of the surface states. **e**, ARPES EDCs of the 3 QL Bi_2Se_3 film measured at 150 K.

Table 1 | Parameters of equations (1) and (2) used to fit the bands in Fig. 2b–e, and the fitted Rashba parameters (α_R).

QL	E_0 (eV)	D (eV \AA^2)	Δ (eV)	B (eV \AA^2)	v_F (10^5 m s^{-1})	$ \tilde{V}' $ (eV)	α_R (eV \AA)
2	-0.470	-14.4	0.252	21.8	4.71	0	0
3	-0.407	-9.7	0.138	18.0	4.81	0.038	0.71
4	-0.363	-8.0	0.070	10.0	4.48	0.053	1.27
5	-0.345	-15.3	0.041	5.0	4.53	0.057	2.42
6	-0.324	-13.0	0	0	4.52	0.068	2.78

the parameters D and B can be found in ref. 15. For a 1 QL film, only one band can be observed. The absence of the lower surface states may be due to the bonding with the substrate. The ARPES spectra of 2 QL can be well fitted by equation (1). The pink dashed lines in Fig. 2b depict the fitted curves with the parameters listed in Table 1. However, starting from 3 QL, the surface states exhibit Rashba-type splitting. The splitting cannot be obtained with equation (1), and neither by previous first-principles calculation¹⁶. Both the effective model and the first-principles calculation are based on a free-standing symmetric topological insulator film, whereas the existence of substrate breaks the structural inversion symmetry, which can result in a Rashba-type spin splitting in the ultrathin-film regime.

To model the substrate effect, we invoke an effective electrical potential $V(z)$ along the film normal direction. From this modified model, we can obtain the dispersions²⁵:

$$E_{\sigma\pm}(k_{\parallel}) = E_0 - Dk_{\parallel}^2 \pm \sqrt{(|\tilde{V}'| + \sigma v_F \hbar k_{\parallel})^2 + \left(\frac{\Delta}{2} - Bk_{\parallel}^2\right)^2} \quad (2)$$

The \tilde{V}' term represents the effect of the potential $V(z)$. Each spin-degenerate dispersion in equation (1) is now split into two

sub-bands of opposite spins ($\sigma = \pm 1$) that shift away from each other along the k_{\parallel} axis. If $\tilde{V}' = 0$, equation (2) degenerates into equation (1), which corresponds to the 2 QL case discussed above. The splitting of the upper surface states is very well reproduced in the fitting with equation (2) (see the dashed lines in Fig. 2c–e). When Δ is zero, the dispersions obtained from equation (2) evolve into two sets of Dirac cones centred at the Γ point. The two Dirac points are shifted in energy by $2|\tilde{V}'|$. In the ARPES data, at 6 QL only one Dirac cone was observed. The outer branches of the Rashba-split upper surface states, which are expected to evolve into part of the other Dirac cone, are nearly invisible. In Fig. 3c, the calculated weights in real space of the surface states at 5 QL are shown with the colours of the lines. It is clear that near critical thickness the outer and inner branches of the Rashba-split surface states localize at different surfaces of the film. The two Dirac cones obtained from equation (2) correspond to the two sets of gapless surface states from the surface and interface sides of the film, respectively. The absence of one Dirac cone in the ARPES spectra is due to its localization at the interface side, which is beyond the detection depth of ARPES. In this context, the observed Rashba splitting can also be understood as a result of the hybridization of the two sets of gapless surface states with different Dirac points from the two surfaces of the film.

The breaking of structural inversion symmetry of the system can originate from the band bending induced by the substrate, as suggested in Fig. 3a, or alternatively from different environments of the two surfaces. In the former case, when the film is much thinner than the thickness of the band-bending region, that is, the Debye length, which is determined by the dielectric constant and carrier density of the material, the potential variation along the z direction of the film will be negligible. So the Rashba effect is weaker in thinner films. In the latter case, the structural asymmetry is more significant in thinner films, and thus the Rashba effect is stronger. Our observation of reduced Rashba splitting with decreasing film thickness suggests that the former case dominates in Bi_2Se_3 films. In an epitaxial film, band bending can be modified by the surface photovoltage (SPV) effect, which takes place in a p–n or Schottky junction in which the photon-excited electrons and holes are driven in opposite directions by a space charge layer^{26,27}. As a result, the band bending is reduced and even completely removed. The SPV effect is more prominent at low temperature because of less electron–hole recombination. The epitaxial Bi_2Se_3 films show a strong SPV effect at 150 K, which is confirmed by the 0.06 eV shift of the Fermi edge compared with the room-temperature spectra²⁶. In Fig. 3e, we show EDCs of ARPES spectra of 3 QL Bi_2Se_3 at 150 K. Rashba splitting cannot be distinguished any more, whereas other features, for example the gap size, are basically similar to the room-temperature data. The thickness dependence of energies of the Dirac point (≥ 6 QL) and mid-gap position (< 6 QL) measured at low temperature is also shown in Fig. 3a. The variation of chemical potential with thickness is largely reduced, suggesting a nearly flat band. The quench of the Rashba splitting by the SPV effect demonstrates that the splitting is mainly contributed by substrate-induced band bending.

The above conclusion implies that the Rashba splitting can be controlled by modifying band bending, which can be easily realized by applying a gate voltage. It is of great significance for spintronic devices, especially the Datta–Das spin field-effect transistor²⁸, in that the spin structure can be tuned electrically. In Table 1, the fitted Rashba parameter α_R values are listed. The Bi_2Se_3 films (3–6 QL) show at least one order of magnitude larger Rashba splitting than semiconductor heterostructures²⁹, and the splitting can be removed by changing the band bending by ~ 0.3 eV. Therefore, ultrathin materials of topological insulators provide a new kind of spintronic materials that may realize high-efficiency electrical spin manipulation.

A thickness-dependent oscillatory transition with a periodicity of 3 QL between QSH and ordinary insulator phases was predicted theoretically¹⁴. The oscillation mostly refers to the sign of the gap, but could also lead to an oscillation in the magnitude of the gap size^{13–15}. In Fig. 3d, we show the measured gap size as a function of thickness, which is more or less monotonic. According to refs 15,25, if Δ and B in equation (2) have the same sign, the film is in the QSH phase, otherwise, it is a trivial insulator. From the fitted parameters listed in Table 1, we can see that from 2 to 5 QL, Δ and B have the same sign. Therefore, it illustrates that the films are in the QSH regime. However, because band dispersion can be influenced by other non-universal factors, further experiments by STM and electrical transport measurement with and without external magnetic field, similar to those carried out in ref. 4, are needed to clarify this issue.

Methods

All experiments were carried out in an ultrahigh-vacuum system (Omicron), equipped with MBE, an STM and ARPES. The base pressure of the system is 1.5×10^{-10} torr. In the ARPES measurement, photoelectrons are excited by an unpolarized He-I α light (21.21 eV), and collected by a Scienta SES-2002 analyser (15 meV). Bi_2Se_3 films were grown under Se-rich conditions on a double-layer-graphene-terminated 6H-SiC (0001) substrate at 220 °C by MBE. Bi (99.9999%) and Se (99.999%) were both evaporated from standard Knudsen

cells. The growth rate was calibrated by a real-time RHEED intensity oscillation measured on the (00) diffraction. The $\text{Se}_4(\text{Se}_2)/\text{Bi}$ flux ratio was between 10 and 15, which leads to a growth rate of ~ 0.3 QL min^{-1} when the Bi source temperature was set at 550 °C.

Received 31 October 2009; accepted 5 May 2010; published online 13 June 2010

References

- Qi, X.-L. & Zhang, S.-C. The quantum spin Hall effect and topological insulators. *Phys. Today* **63**, 33–38 (2010).
- Hasan, M. Z. & Kane, C. L. Topological insulators. Preprint at <http://arxiv.org/abs/1002.3895> (2010).
- Bernevig, B. A., Hughes, T. L. & Zhang, S.-C. Quantum spin Hall effect and topological phase transition in HgTe quantum wells. *Science* **314**, 1757–1761 (2006).
- König, L. M. *et al.* Quantum spin Hall insulator state in HgTe quantum wells. *Science* **318**, 766–770 (2007).
- Fu, L., Kane, C. L. & Mele, E. J. Topological insulators in three dimensions. *Phys. Rev. Lett.* **98**, 106803 (2007).
- Hsieh, D. *et al.* A topological Dirac insulator in a quantum spin Hall phase. *Nature* **452**, 970–974 (2008).
- Qi, X.-L., Hughes, T. L. & Zhang, S.-C. Topological field theory of time-reversal invariant insulators. *Phys. Rev. B* **78**, 195424 (2008).
- Hsieh, D. *et al.* Observation of unconventional quantum spin textures in topological insulator. *Science* **323**, 919–922 (2009).
- Nishide, A. *et al.* Direct mapping of the spin-filtered surface bands of a three-dimensional quantum spin Hall insulator. *Phys. Rev. B* **81**, 041309(R) (2010).
- Žutić, I., Fabian, J. & Das Sarma, S. Spintronics: Fundamentals and applications. *Rev. Mod. Phys.* **76**, 323–410 (2004).
- Nayak, C. *et al.* Non-abelian anyons and topological quantum computation. *Rev. Mod. Phys.* **80**, 1083–1159 (2008).
- Moore, J. Topological insulators: The next generation. *Nature Phys.* **5**, 378–380 (2009).
- Linder, J., Yokoyama, T. & Sudbø, A. Anomalous finite size effects on surface states in the topological insulator Bi_2Se_3 . *Phys. Rev. B* **80**, 205401 (2009).
- Liu, C.-X. *et al.* Oscillatory crossover from two dimensional to three dimensional topological insulators. *Phys. Rev. B* **81**, 041307(R) (2010).
- Lu, H.-Z. *et al.* Massive Dirac fermions and spin physics in an ultrathin film of topological insulator. *Phys. Rev. B* **81**, 115407 (2010).
- Zhang, H. J. *et al.* Topological insulators in Bi_2Se_3 , Bi_2Te_3 and Sb_2Te_3 with a single Dirac cone on the surface. *Nature Phys.* **5**, 438–442 (2009).
- Xia, Y. *et al.* Observation of a large-gap topological-insulator class with a single Dirac cone on the surface. *Nature Phys.* **5**, 398–402 (2009).
- Hsieh, D. *et al.* A tunable topological insulator in the spin helical Dirac transport regime. *Nature* **460**, 1101–1105 (2009).
- Chen, Y. L. *et al.* Experimental realization of a three-dimensional topological insulator, Bi_2Te_3 . *Science* **325**, 178–181 (2009).
- Zhang, G. *et al.* Quintuple-layer epitaxy of thin films of topological insulator Bi_2Se_3 . *Appl. Phys. Lett.* **95**, 053114 (2009).
- Peng, H. *et al.* Aharonov–Bohm interference in topological insulator nanoribbons. *Nature Mater.* advance online publication, doi:10.1038/nmat2609 (13 December 2009).
- Zhou, B. *et al.* Finite size effects on helical edge states in a quantum spin–Hall system. *Phys. Rev. Lett.* **101**, 246807 (2008).
- Hor, Y. S. *et al.* p-type Bi_2Se_3 for topological insulator and low-temperature thermoelectric applications. *Phys. Rev. B* **79**, 195208 (2009).
- Chiang, T.-C. Photoemission studies of quantum well states in thin films. *Surf. Sci. Rep.* **39**, 181–235 (2000).
- Shan, W.-Y., Lu, H.-Z. & Shen, S.-Q. Effective continuous model for surface states and thin films of three-dimensional topological insulators. *New J. Phys.* **12**, 043048 (2010).
- Demuth, J. E. *et al.* Photoemission-based photovoltage probe of semiconductor surface and interface electronic structure. *Phys. Rev. Lett.* **56**, 1408–1411 (1986).
- Alonso, M., Cimino, R. & Horn, K. Surface photovoltage effects in photoemission from metal–GaP (110) interfaces: Importance for band bending evaluation. *Phys. Rev. Lett.* **64**, 1947–1950 (1990).
- Datta, S. & Das, B. Electronic analog of the electro-optic modulator. *Appl. Phys. Lett.* **56**, 665–667 (1990).
- Ast, C. R. *et al.* Giant spin splitting through surface alloying. *Phys. Rev. Lett.* **98**, 186807 (2007).

Acknowledgements

This work was supported by the National Science Foundation and Ministry of Science and Technology of China and RGC of Hong Kong, China under grant No. HKU

7037/08P. X-L.Q., S-C.Z. and Q.N. are supported by the Department of Energy, Office of Basic Energy Sciences, Division of Materials Sciences and Engineering, under contracts DE-AC02-76SF00515 and DE-FG03-02ER45958.

Author contributions

K.H., S-Q.S., X-C.M. and Q-K.X. conceived and designed the experiments. Y.Z., K.H. and C-Z.C. carried out MBE growth and ARPES measurements. C-L.S. carried out substrate preparation and STM observation. L-L.W., X.C., J-F.J., X-C.M. and Q-K.X. assisted

in the experiments. W-Y.S. and S-Q.S. carried out the theoretical analyses and data interpretations. Q.N., Z.F., X.D., X-L.Q. and S-C.Z. assisted in the theoretical analyses. Y.Z., K.H., S-Q.S., S-C.Z. and Q-K.X. prepared the manuscript.

Additional information

The authors declare no competing financial interests. Reprints and permissions information is available online at <http://npg.nature.com/reprintsandpermissions>. Correspondence and requests for materials should be addressed to K.H. or Q-K.X.

Yi Zhang¹, Ke He^{1*}, Cui-Zu Chang^{1,2}, Can-Li Song^{1,2}, Li-Li Wang¹, Xi Chen², Jin-Feng Jia², Zhong Fang¹, Xi Dai¹, Wen-Yu Shan³, Shun-Qing Shen³, Qian Niu⁴, Xiao-Liang Qi⁵, Shou-Cheng Zhang⁵, Xu-Cun Ma¹ and Qi-Kun Xue^{1,2*}

¹Institute of Physics, Chinese Academy of Sciences, Beijing 100190, China, ²Department of Physics, Tsinghua University, Beijing 100084, China, ³Department of Physics and Center for Theoretical and Computational Physics, The University of Hong Kong, Pokfulam Road, Hong Kong, China, ⁴Department of Physics, The University of Texas, Austin, Texas 78712-0264, USA, ⁵Department of Physics, Stanford University, Stanford, California 94305-4045, USA. *e-mail: kehe@aphy.iphy.ac.cn; qkxue@mail.tsinghua.edu.cn.